Initial Experiments and Analysis of Blunt-Edge Vortex Flows

James M. Luckring[1]
NASA Langley Research Center, Hampton, VA, 23681

A review is presented of the initial experimental results and analysis that formed the basis the Vortex Flow Experiment 2 (VFE-2). The focus of this work was to distinguish the basic effects of Reynolds number, Mach number, angle of attack, and leading edge bluntness on separation-induced leading-edge vortex flows that are common to slender wings. Primary analysis is focused on detailed static surface pressure distributions, and the results demonstrate significant effects regarding the onset and progression of leading-edge vortex separation.

Nomenclature

b	=	wing span
d	=	sting diameter
C_L	=	Lift coefficient
C_m	=	Pitching moment coefficient (referenced to (2/3) c_r and based upon mac)
C_N	=	Normal force coefficient
C_p	=	pressure coefficient
C_p^*	=	sonic pressure coefficient
c	=	chord
c_r	=	root chord
E	=	Young's modulus
LTPT	=	Low Turbulence Pressure Tunnel
M, M_∞	=	free-stream Mach number
mac	=	mean aerodynamic chord, (2/3) c_r
NTF	=	National Transonic Facility
q_∞	=	free stream dynamic pressure
R_{mac}	=	Reynolds number, based on mean aerodynamic chord
r_{le}	=	streamwise leading-edge radius
t	=	wing thickness
VFE-2	=	Vortex Flow Experiment 2
x,y,z	=	Cartesian coordinate system
x_v	=	longitudinal distance to vortex separation
α	=	angle of attack, degrees
β	=	Prandtl-Glauert compressibility factor, $[1-(M_\infty)^2]^{1/2}$
η	=	non-dimensional local semispan
Λ	=	Leading-edge sweep, degrees

I. Introduction

In the early 1980's expanded planning was undertaken to develop models and test programs[1,2] for the National Transonic Facility (NTF) at NASA Langley Research Center. The models spanned research distinctions from fundamental to configuration concepts. The test programs for the most part addressed combinations of Reynolds number effects and high Reynolds number aerodynamics for attached and separated flows at subsonic or transonic speeds.

[1] Senior Research Engineer, Configuration Aerodynamics Branch, Mail Stop 499, AIAA Associate Fellow.

One of these programs was focused on separation-induced leading-edge vortex flows from slender wings with blunt leading edges. Various aerodynamic and testing considerations led to the selection of a 65° swept delta wing for the basic geometry. The wing supported testing with different leading-edge components as a means to vary the leading-edge bluntness. Maneuvering aircraft develop these flows with blunt-edge separation, and thus it was felt that this program would extend the previous knowledge obtained with sharp-edged delta wings in a useful manner.

This test program was executed in the early 1990's along with a companion experiment in the Low Turbulence Pressure Tunnel (LTPT), and first data analysis of the NTF data[3-6] was published[2,7-10] in the early 2000's. The analyses not only demonstrated significant effects of the parameters investigated, but also indicated a new structure to the leading-edge vortex separation from the blunt edges that did not occur with sharp leading edges. Discussions and further analysis[11] led to the proposal[12] for an international research campaign that became known as Vortex Flow Experiment 2 (VFE-2).

In this paper a brief review is presented of the knowledge leading up to the beginning of VFE-2. Results are included from a number of the author's previous publications along with analysis of some new results.

II. Basic considerations for slender-wing vortex flows

Many overall characteristics of vortex flows for the sharp-edged and highly-swept delta wing have been established[13,14]. For this case, the flow undergoes a primary separation at the wing leading edge and subsequently rolls up to form a stable, separation-induced leading-edge vortex over the wing. A sketch of this vortex, from Hummel[13], is shown in **Fig. 1**. The primary vortex induces reattached flow over the wing, and the spanwise flow under the primary vortex subsequently separates a second time to form a counter-rotating secondary vortex outboard of the primary vortex. The flow under the vortices induces significant upper surface suction pressures that can result in large vortex-induced lift increments at moderate to high angles of attack. An example of these lift increments is also shown in Fig. 1 along with theoretical estimates of the vortex lift due to Polhamus[14].

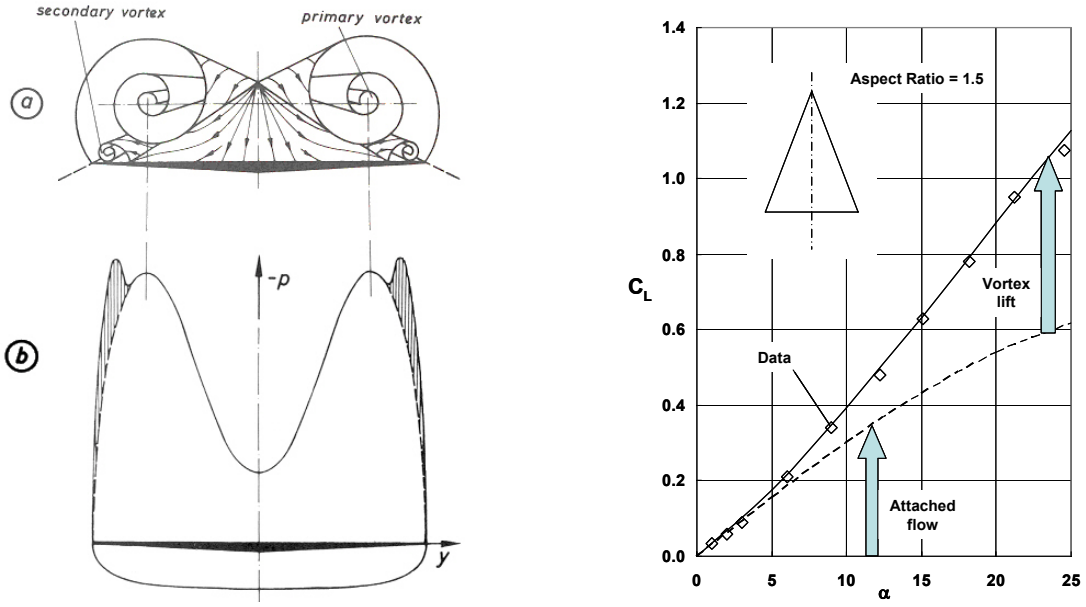

Hummel[13] Polhamus[14]

Figure 1. Some basic features of separation-induced leading-edge vortex flows for sharp-edged delta wings.

The blunt leading edge fundamentally alters this flow (**Fig. 2**). The origin of the vortex will be displaced from the apex of the delta wing, and any leading-edge vortex separation will occur from a location near, but not necessarily at, the leading edge. Moreover, the onset and progression of the vortex separation will be a function of the flow conditions and wing geometry. For example, at low to moderate angles of attack the wing could exhibit fully attached flow. As angle of attack is increased, leading-edge separation will first occur at a location near the trailing edge for two reasons. First, delta wing leading-edge upwash distributions increase from the apex to the trailing edge, and thus the local angle of attack is higher near the trailing edge. Second, the crossflow bluntness

(r_{le}/b_{loc}) tends to progress from blunter to sharper values as the trailing edge is approached. With further angle of attack increases the onset of this vortex separation will progress longitudinally up the leading edge. Thus, for some angle-of-attack range the wing will exhibit partial span leading-edge vortex separation with attached flow on the upstream portion of the wing and leading edge vortex separation on the downstream portion. Because the leading-edge vortex separation is now occurring from a smooth surface, the physics of this flow could be quite different from the sharp-edged case, and the strength, position, and the very existence of the vortex will be affected by leading-edge radius and will change with Mach number, Reynolds number, and angle of attack.

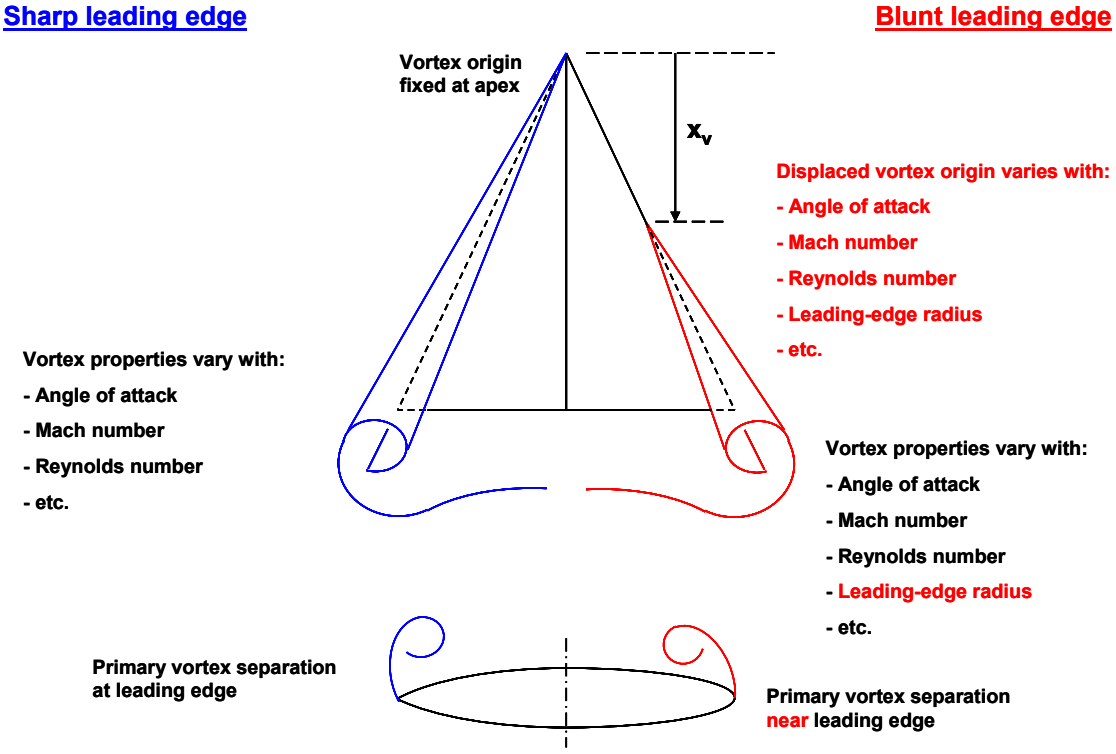

Luckring[10]

Figure 2. Leading-edge bluntness consequences for the primary vortex separation.

III. Models and Tests

The wind tunnel model and test programs were designed to quantify the independent effects of Mach number, Reynolds number, angle of attack, and leading edge bluntness on the onset and progression of leading edge vortex separation.

Some basic characteristics of the model are summarized in **Fig 3**. The 65° delta wing had no twist or camber and had interchangeable leading-edge segments that incorporated the various leading-edge radii. The central portion of the wing was flat. With this approach, the new blunt-edged delta wing data would relate to previous data bases developed with flat-plate sharp-edged delta wings. The wind tunnel model was designed to generate delta-wing aerodynamics with minimal wind-tunnel test interference effects.

The leading-edge contours had a NACA-like polynomial form with a single parameter, the leading edge bluntness. See **Fig. 4**. The contours matched the inner flat-plate portion of the wing with continuity through second derivative and, hence, curvature. This continuity is of course crucial to avoid unintended separation artificially induced by the model. The bluntness values were selected to be practical as regards values used for maneuvering aircraft and included a sharp leading edge (r_{le}=0) within the same functional family.

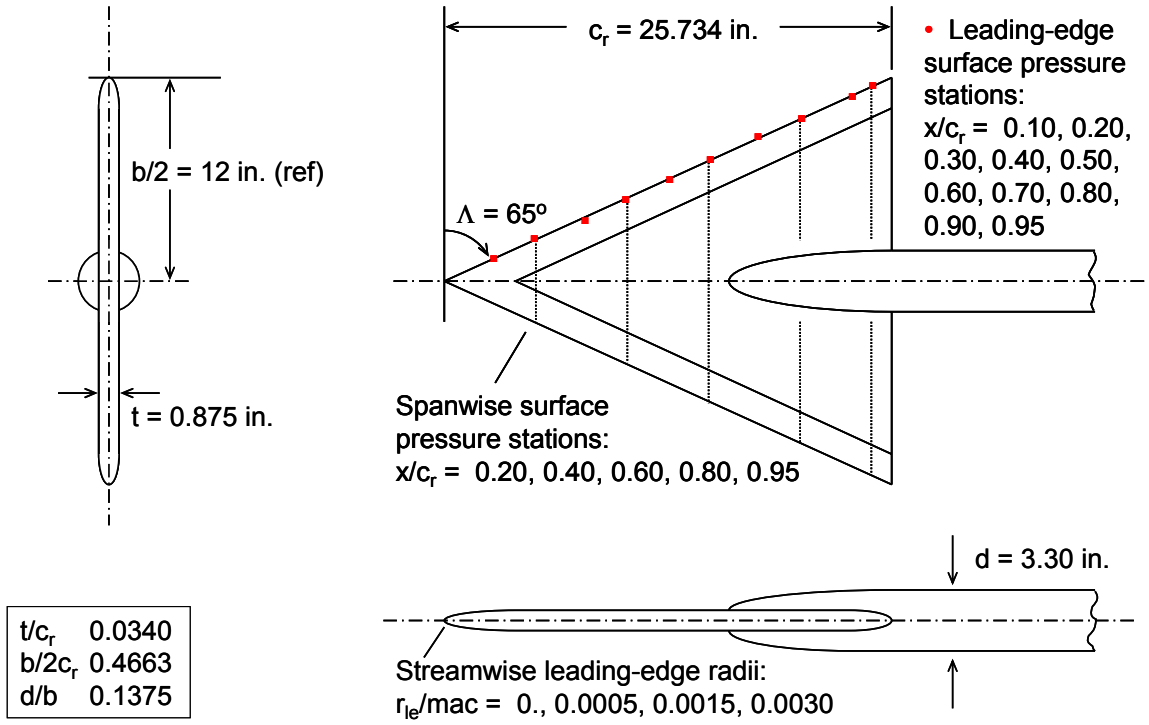

Figure 3. Delta wing configuration for tests in NTF.

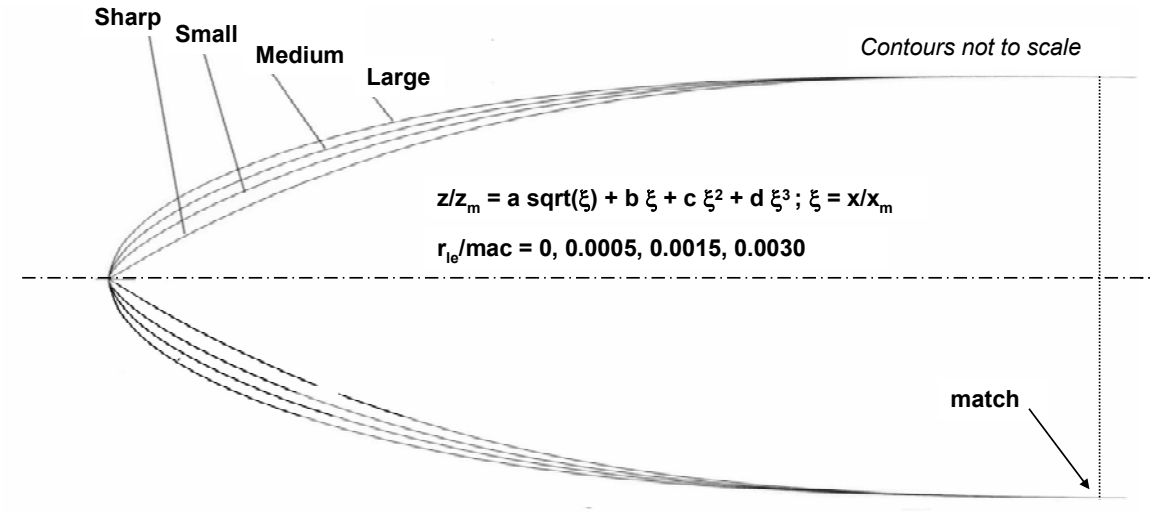

Figure 4. Leading-edge geometry.

The emphasis for the experiment was on static surface pressure measurements, and for most configurations there were approximately 183 pressure taps organized along constant percent local semispan locations at constant percent root-chord stations. Pressure taps were also situated directly on the leading edge (i.e., η=1) to facilitate separation onset measurement. Because of the extensive pressure instrumentation, there was no room in the model for a conventional internal strain-gauge balance. However, the sting itself was gauged to provide measurement on normal force and pitching moment.

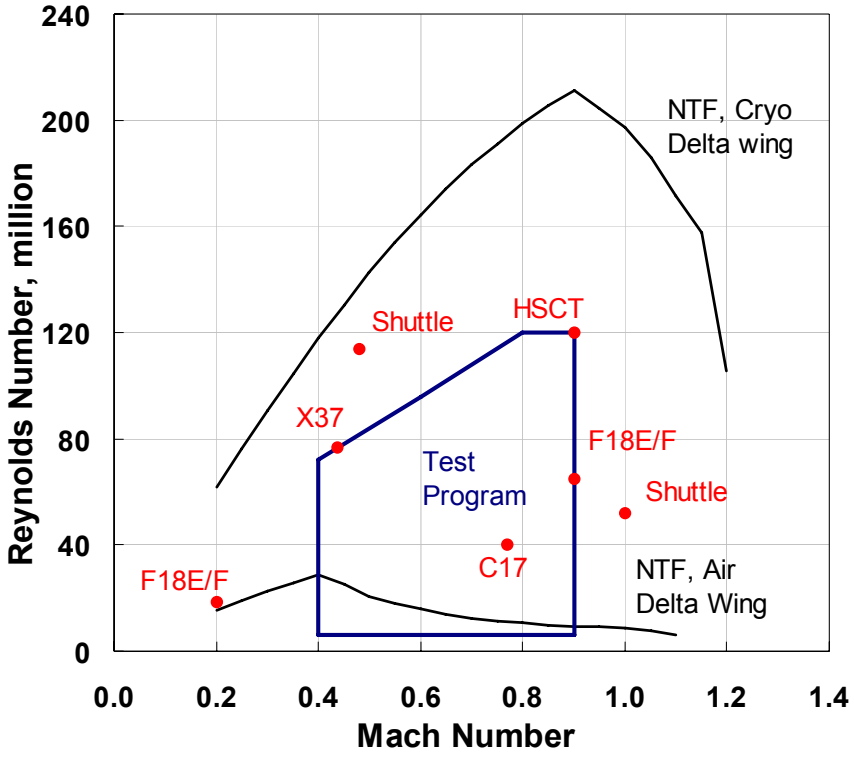

Figure 5. National Transonic Facility test program.

Primary experiments were performed in the National Transonic Facility[15,16] (NTF) at the NASA Langley Research Center. This tunnel allows for independent control of Mach number (0.1 to 1.2), total pressure (1.2 atm to 8.8 atm), and total temperature (-250 F to 120 F) through the injection of cryogenic nitrogen. The test section is slotted and 8.2 feet square.

Through the combination of pressure and cryogenic temperatures the NTF can test at very high Reynolds numbers. Because the tunnel has three degrees of freedom in operation conditions (speed, total pressure and total temperature), it can also be used to vary one free-stream parameter while holding two other free-stream parameters constant. For example, free-stream Reynolds number can be varied while holding Mach number (compressibility effects) and q_∞/E (aeroelastic effects) constant. This feature can be exploited for other means as well, say to vary Mach number while holding Reynolds number and q_∞/E constant. Thus, Reynolds number, Mach number, and aeroelastic effects can be isolated experimentally.

The facility operation envelope for the NTF delta wing along with the range of the delta wing experimental program is shown in **Fig 5**. The range of test conditions were chosen to be representative of operating conditions for a variety of aircraft incorporating slender-wing flows; transonic cruise conditions for a representative military transport (C17) and a conceptual High Speed Civil Transport (HSCT) are also shown for reference.

The tests were designed to minimize potential data contaminants including those often referred to as pseudo Reynolds number effects. The wing was hydraulically smooth ($k^+<5$) for the range of Reynolds numbers investigated. Wing design analysis indicated negligible aeroelastic effects. An offset sting kept the model on the tunnel centerline for the angle-of-attack range investigated. In addition, wind tunnel wall interference was believed to be negligible based on established best practices for the slotted-wall test section (e.g., the model span relative to the tunnel width, model area relative to the tunnel cross sectional area, model positioning).

The gauging requirements for the high loads encountered in the NTF test campaign precluded acceptable measurement accuracies at test conditions below a free-stream Mach number of 0.4. To obtain lower speed data, a second wing was designed for testing in the Low Turbulence Pressure Tunnel[17] (LTPT) located at the NASA Langley Research Center. The test conditions were focused at a free-stream Mach number of 0.2, and Reynolds numbers were varied between 2×10^6 and 12×10^6. The model was a ¾ scale version of the NTF delta wing model.

This size was determined[18,19] to provide correctable wall-interference effects. A comparison of the two models in their respective test sections is shown in **Fig. 6**.

Figure 6. LTPT and NTF delta wings.

IV. Aerodynamics of blunt-edged vortex flows

A contrast between sharp-edged and blunt-edged vortex flow results is presented first. These results are followed by a discussion of Reynolds number effects for the varying leading-edge bluntness values. Mach number effects are presented next followed by some discussion of the significance of isolating these effects.

A. Contrast of sharp and blunt edge flows

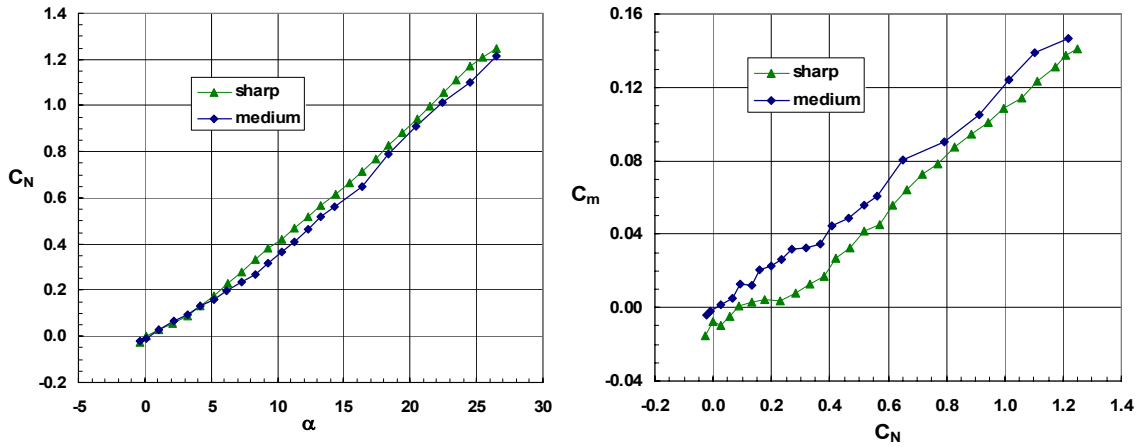

Figure 7. Effect of leading-edge bluntness on normal force and pitching moment coefficients. Sharp and medium bluntness leading edges, $M_\infty = 0.4$, $R_{mac} = 6 \times 10^6$. Data from NTF.

A comparison between the sharp and medium bluntness leading-edge configurations is presented in **Fig. 7** for the normal force and pitching moment coefficients at a free-stream Mach number of 0.4 and a free-stream Reynolds number of 6 million. The blunt leading edge separation weakens the vortex compared to the sharp leading edge case, and the normal force coefficient is reduced from the sharp-edged values for the angle of attack range investigated.

Pitching moment results show the blunt-edged wing to have a more forward (i.e., toward the wing apex) center of pressure than the sharp-edged case. Leading-edge vortex loadings tend to be situated further aft than attached

flow loadings, and thus this forward shift in pitching moment is consistent with the reduced vortex strength from the blunt leading edge.

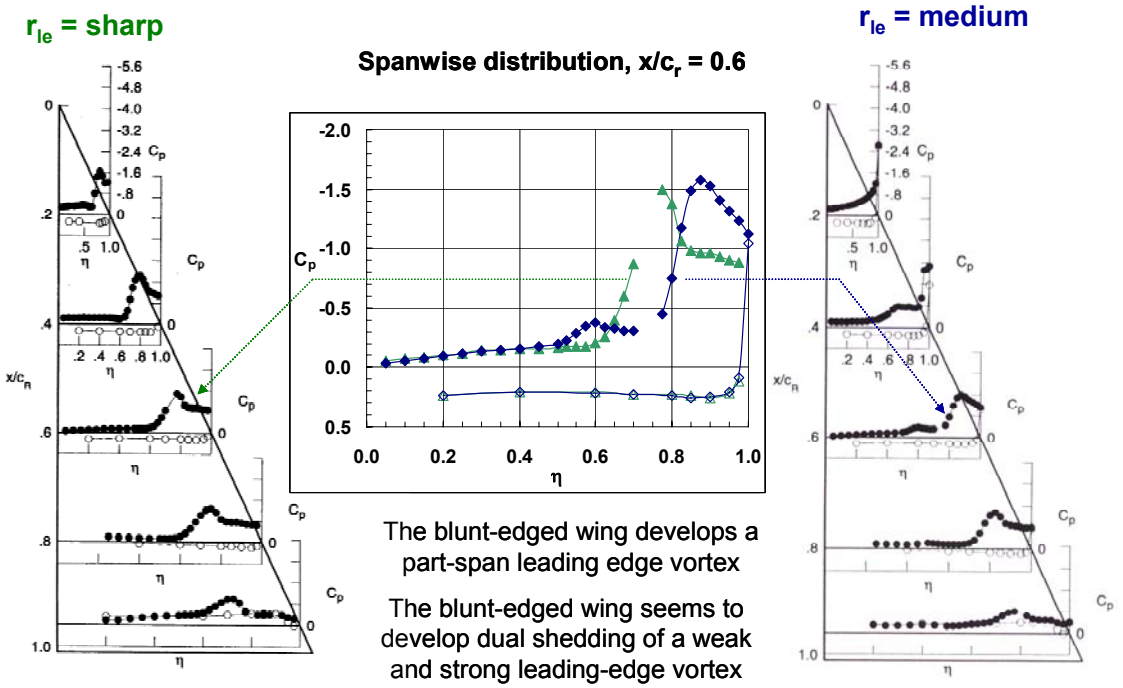

Figure 8. Static surface pressure coefficients for medium bluntness delta wing. $\alpha = 13^o$, $M_\infty = 0.4$, $R_{mac} = 6 \times 10^6$. Data from NTF.

A comparison of the static surface pressure coefficients for the sharp-edged and medium bluntness delta wing is shown in **Fig. 8** for a nominal angle of attack of 13°. The sharp-edged wing exhibits typical separation-induced leading-edge vortex properties. The primary vortex suction peak is situated conically on the wing and diminishes in magnitude as the trailing edge is approached. At this moderate angle of attack vortex breakdown does not occur in the vicinity of the wing, and this drop in primary vortex suction is due to the trailing-edge Kutta condition in conjunction with longitudinal vortex curvature effects. Outboard of this suction peak turbulent secondary separation is also indicated.

The blunt-edged delta wing surface pressure coefficients clearly demonstrate part span leading-edge vortex separation, Fig. 8. Attached flow pressures are evident at 20% root chord while leading-edge vortex-like pressures are evident from 60% root chord aft. The origin of the blunt leading-edge vortex for this case is in the vicinity of 30% root chord. This class of leading-edge vortex separation does not exist for corresponding flat-plate sharp-edged wings. The direct comparison of the pressures in Fig. 8 at 60% root chord demonstrates the outboard shift of the vortex footprint due to leading-edge bluntness.

The pressures at 60% root chord station also indicate a second suction peak near 60% local semispan. This is inboard of the primary suction peak and may indicate a second co-rotating primary vortex shed from the blunt leading edge. This was also a new feature for the blunt leading edge vortex separation as compared to the sharp edge case. Two sketches of this postulated flow structure of these vortices are presented below in **Fig. 9** from private discussions[11]. Co-rotating vortices can be sensitive to their relative strength and position, and small differences (flow, geometry, etc.) could result in the vortices either developing separate and roughly streamwise trajectories or developing a mutually intertwined trajectory. Such details are difficult to discern from the static surface pressures.

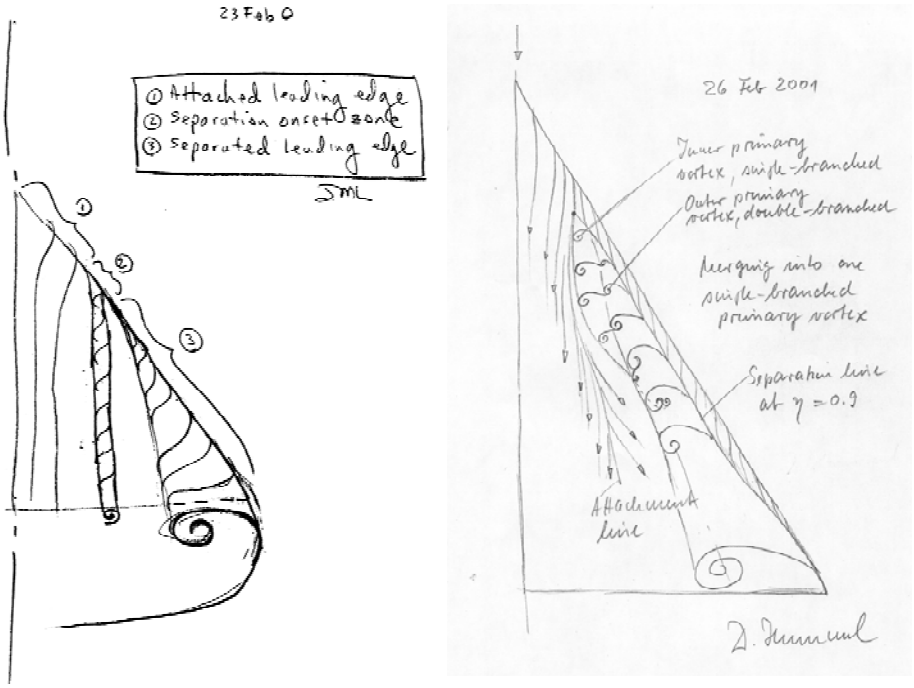

Figure 9. Sketches of blunt leading-edge dual co-rotating leading-edge vortex separation[11].

The details of the flow leading up to the primary vortex separation, with an inner and an outer co-rotation vortex also are curious. The pressures at 40% root chord in Fig. 8 exhibit neither a customary attached flow nor a conventional vortex flow trend. It is unclear if the inner vortex separation is initiated upstream and then triggered by the outer primary separation or if the inner and outer vortex separation occurs in a more tightly coupled fashion.

B. Reynolds number and bluntness effects

Reynolds number effects for a variety of constant Mach numbers were determined for all leading edges of the test program in both the NTF and the LTPT facilities. In this section Reynolds number effects on the static surface pressure coefficients and on the inferred onset and progression of leading-edge vortex separation will be reviewed.

The effect of Reynolds number on the blunt leading edge vortex flow is summarized in **Fig. 10**. Results on the left portion of this figure are the same ones used in Fig. 8 to compare with sharp-edged flow. Comparison of these results at R_{mac} = 6 million (typical of wind-tunnel conditions) to those at 60 million (representative of flight conditions) show significant recovery of attached flow at the higher Reynolds number. The origin of the leading-edge vortex separation has shifted downstream in association with the higher Reynolds number.

Leading-edge pressures provide a useful means to identify the passage of leading-edge vortex separation onset (see **Fig. 11**). At low angles of attack the leading-edge pressure will follow a trend that can be deduced from attached-flow slender wing theory as $C_{p,le} = C_0 - C_2 \sin^2\alpha$ where C_0 and C_2 are constants, obtained in this case from a fit to the data at low angles of attack. Analyses of the NTF data have demonstrated that this trend is sustained as angle of attack is increased and departure from this trend correlates with separation onset[7-9].

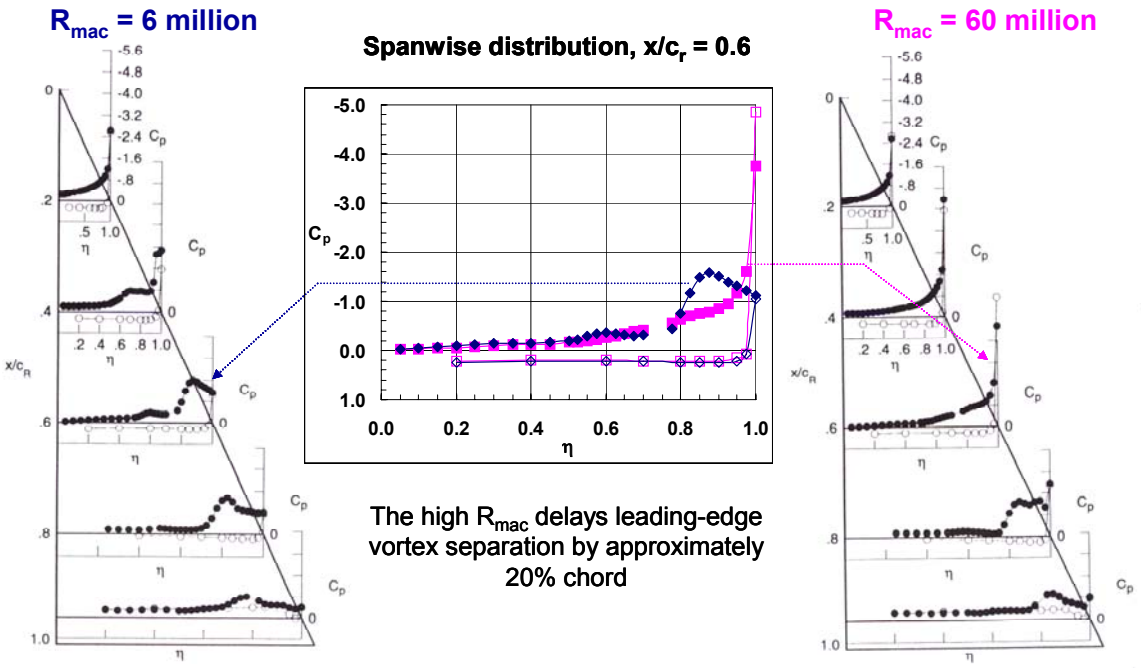

Figure 10. Effect of Reynolds number on static surface pressure coefficients. Medium bluntness, $\alpha = 13^o$, $M_\infty = 0.4$, $R_{mac} = 6 \times 10^6$ and 60×10^6. Data from NTF.

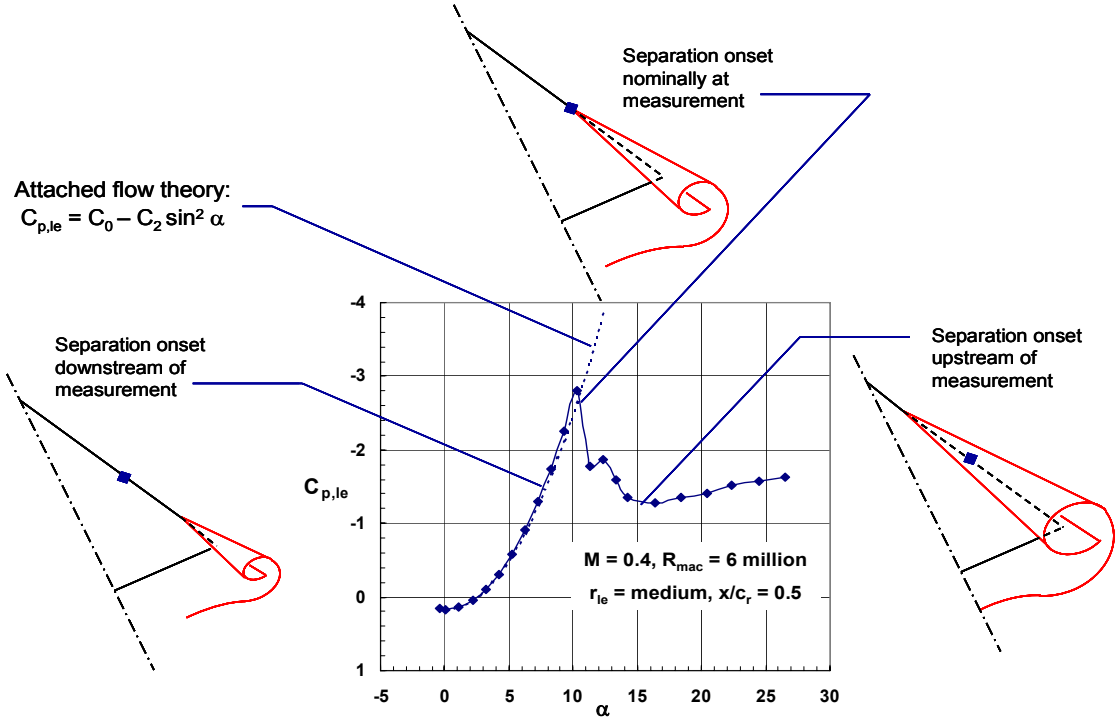

Figure 11. Correlation of leading-edge pressure coefficients with the onset and progression of leading-edge vortex separation. Medium bluntness, $M_\infty = 0.4$, $R_{mac} = 6 \times 10^6$. Data from NTF.

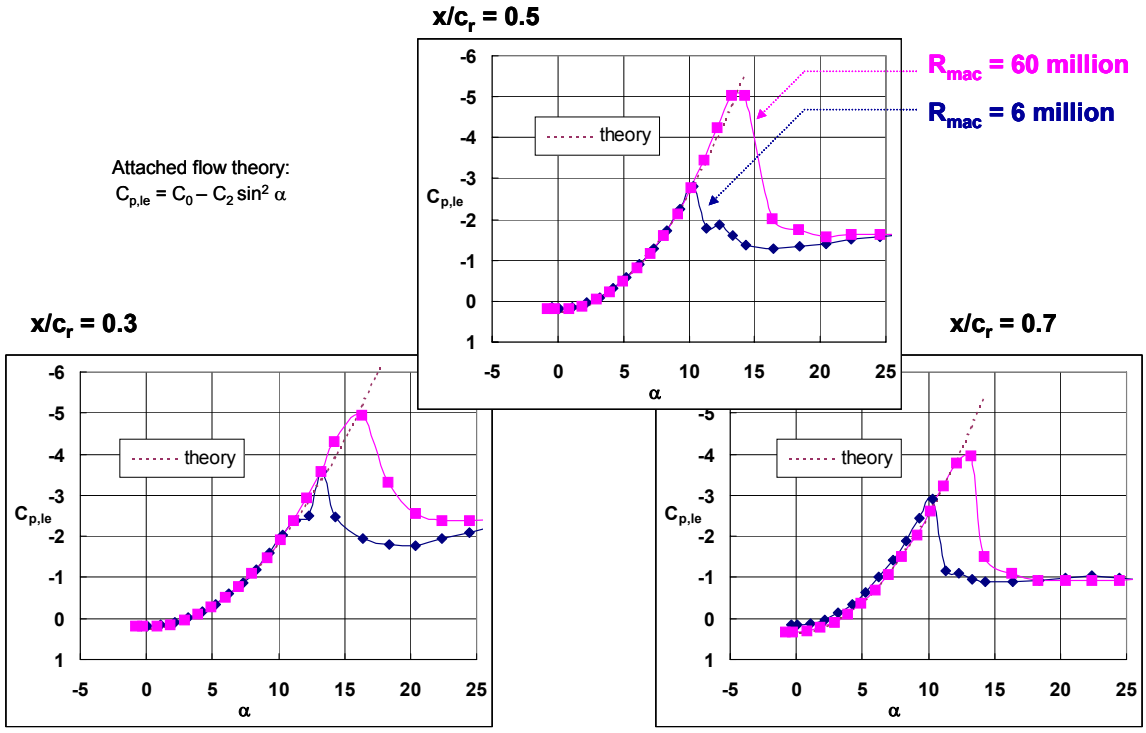

Figure 12. Reynolds number effect on leading-edge pressures. Medium bluntness, $M_\infty = 0.4$.

The leading-edge pressures can be used to assess the effects of various parameters on leading-edge separation. An example is given in **Fig. 12**. Here Reynolds number is shown to delay separation at three root chord stations. Reynolds number effects occur over a significant angle of attack range at values typical of maneuver conditions. The Reynolds number effects also persist over a greater angle of attack range on the forward portions of the wing.

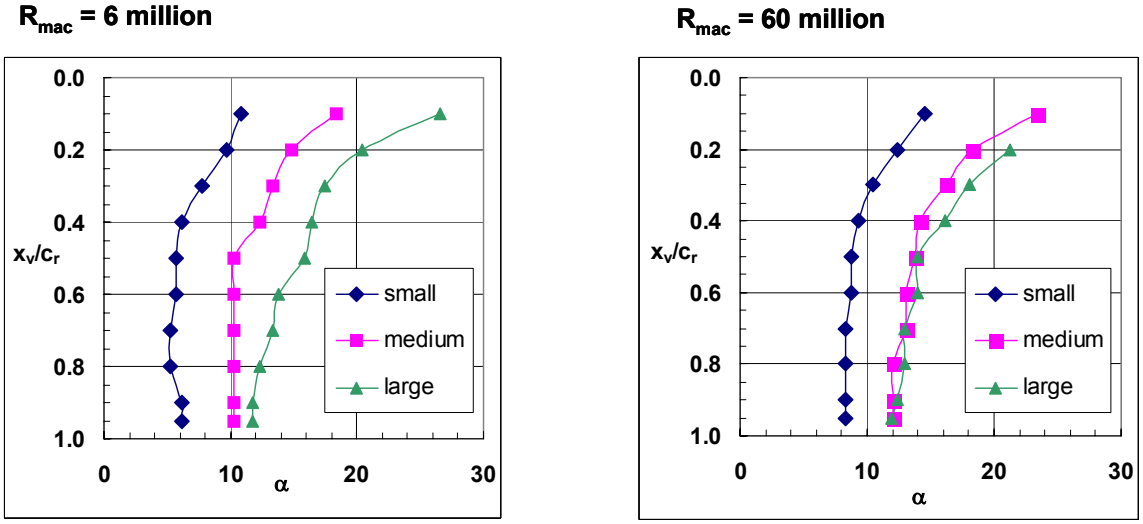

Figure 13. Leading-edge bluntness and Reynolds number effects on the onset and progression of leading-edge vortex separation. $M_\infty = 0.4$.

A summary of leading-edge bluntness effects on the onset and progression of leading-edge separation at low and high Reynolds numbers is presented in **Fig. 13**. At the low Reynolds number the smallest leading-edge bluntness

delayed separation onset to approximately 6 degrees angle of attack. Both the medium and the large bluntness values further delayed separation onset. The largest bluntness showed a gradual progression of separation compared to the other two blunt leading edges. At high Reynolds number separation onset for the small and medium bluntness values has been delayed by about 2 degrees, and separation progression appears to be more gradual. Reynolds number had little effect on the bluntest leading edge. It must be noted that there is most likely some additional uncertainty associated with the results the results of Fig. 13 because they are obtained by inference from the leading edge pressure distributions as opposed to being obtained by direct measurement (say, from surface flow visualization).

C. Compressibility effects

Data	M_∞	R_{mac}
NTF	0.6	6×10^6
NTF	0.4	6×10^6
LTPT	0.2	8×10^6

Linear Prandtl-Glauert compressibility

$$\beta^2 = 1 - M_\infty^2$$

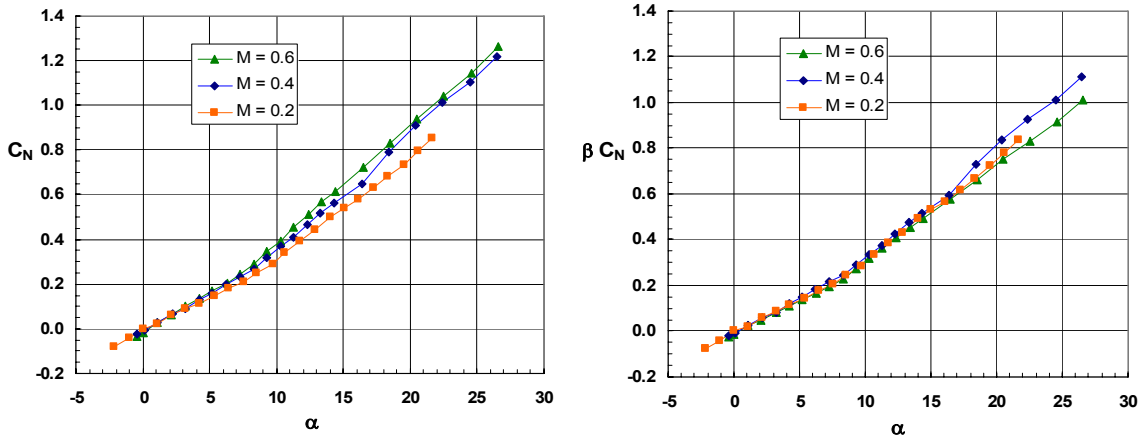

Figure 14. Effect of compressibility on normal force coefficients. Medium bluntness. Data from NTF, LTPT.

The effects of compressibility on the normal force coefficient are shown in **Fig. 14** for the medium bluntness configuration. Results are included from both the NTF and the LTPT experiments. Data from LTPT were not available at the identical Reynolds number as the data from NTF, but it is felt that any Reynolds number effect of this slight mismatch (6 million as compared to 8 million) should be small. For example, at these conditions the zero pressure gradient transition distance differs by only 1.4 percent root chord, and this transition would occur within the first 6 percent root chord from the apex.

The primitive variable data (C_N) demonstrate expected compressibility trends, namely the increase of normal force slope as Mach number is increased. To more clearly assess this effect, similarity scaled results are also shown (βC_N) where the scaling is based upon linear Prandtl-Glauert theory. By this theory the data would be expected to collapse under conditions dominated by small perturbations and hence the linear Prandtl-Glauert governing equation. This would coincide with small angles of attack, and the collapse of the data is very good at low to moderate angles of attack. At the higher angles of attack the flow includes nonlinear effects in association with the leading-edge vortex, and this can also be seen in the scaled results of Fig. 14.

To further assess the compressibility effects, a comparison among static surface pressure coefficients is presented in **Fig. 15** at a nominal angle of attack of 7^o at one chordwise station for this same wing. At these conditions the flow is still attached, and the Prandtl-Glauert similarity scaling would be expected to hold under the same caveats just mentioned in association with Fig. 14. Although not as compelling as the force data, the collapse of the pressure data is good over most of the station shown. The largest mismatch among the scaled results is near the leading edge for the highest Mach number of the comparisons for which the small perturbation assumption is expected to be less valid.

Data	M_∞	R_{mac}	α
NTF	0.6	6 x 10^6	7.3
NTF	0.4	6 x 10^6	7.3
LTPT	0.2	8 x 10^6	7.5

Linear Prandtl-Glauert compressibility

$\beta^2 = 1 - M_\infty^2$

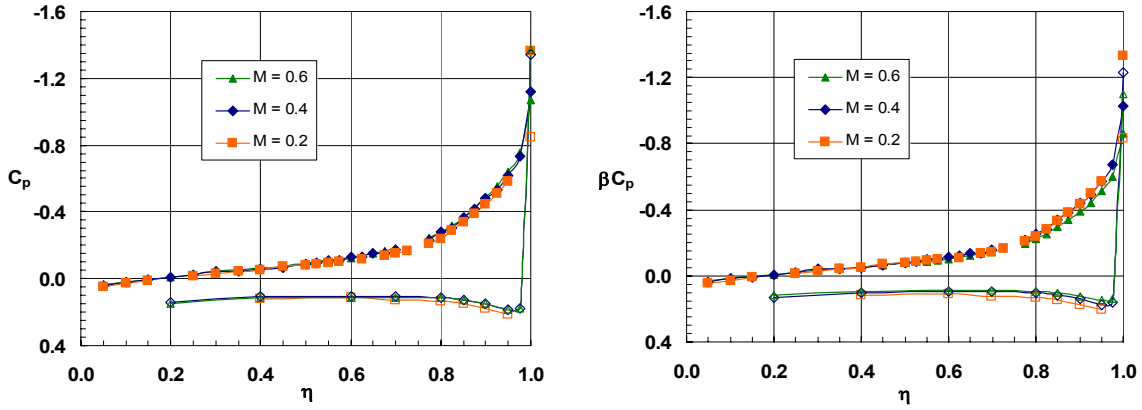

Figure 15. Effect of compressibility on static surface pressure coefficients. Medium bluntness, $x/c_r = 0.6$, $\alpha = 7^o$, data from NTF, LTPT.

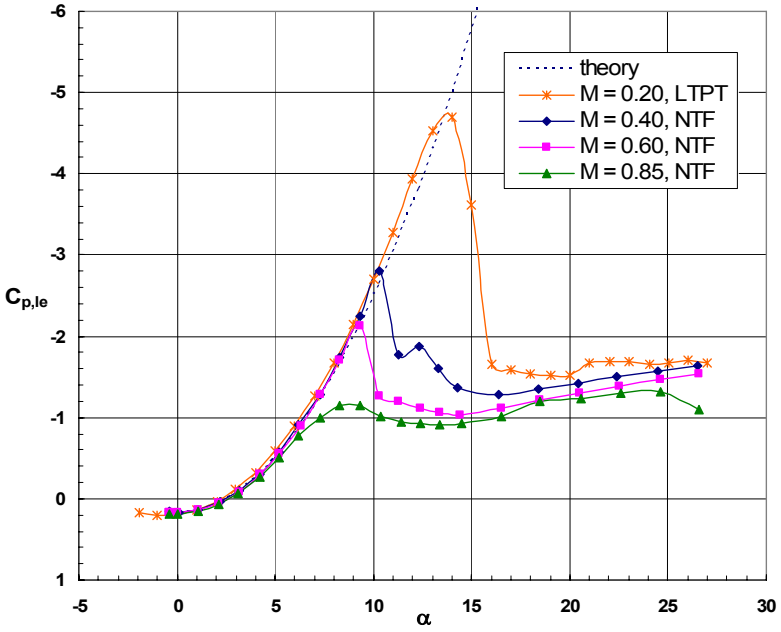

Figure 16. Compressibility effect on leading-edge pressures. Medium bluntness, $x/c_r = 0.5$, $R_{mac} = 6 \times 10^6$, data from NTF, LTPT.

The leading-edge pressure coefficients were shown previously to be useful in inferring onset and progression of leading-edge vortex separation including assessment of Reynolds number and leading-edge bluntness effects. The effect of compressibility on the leading-edge pressure coefficient is shown in **Fig. 16** at the same mid-chord station as before and for a fixed Reynolds number of 6 million. Data are included from both the NTF and the LTPT experiments.

The data demonstrate that the trend with increasing Mach number is to promote departure of the data from attached flow theory and, hence, to promote leading-edge vortex separation. The leading edge flow includes nonlinear contributions since, in general, the perturbations will not be small in this region and, in particular, the onset and progression of leading-edge vortex separation is itself a nonlinear phenomenon. Thus, the correlation between the NTF and the LTPT measurements in terms of exhibiting consistent trends is very encouraging. Additional analysis of the LTPT results for the other leading edges configurations would be of interest.

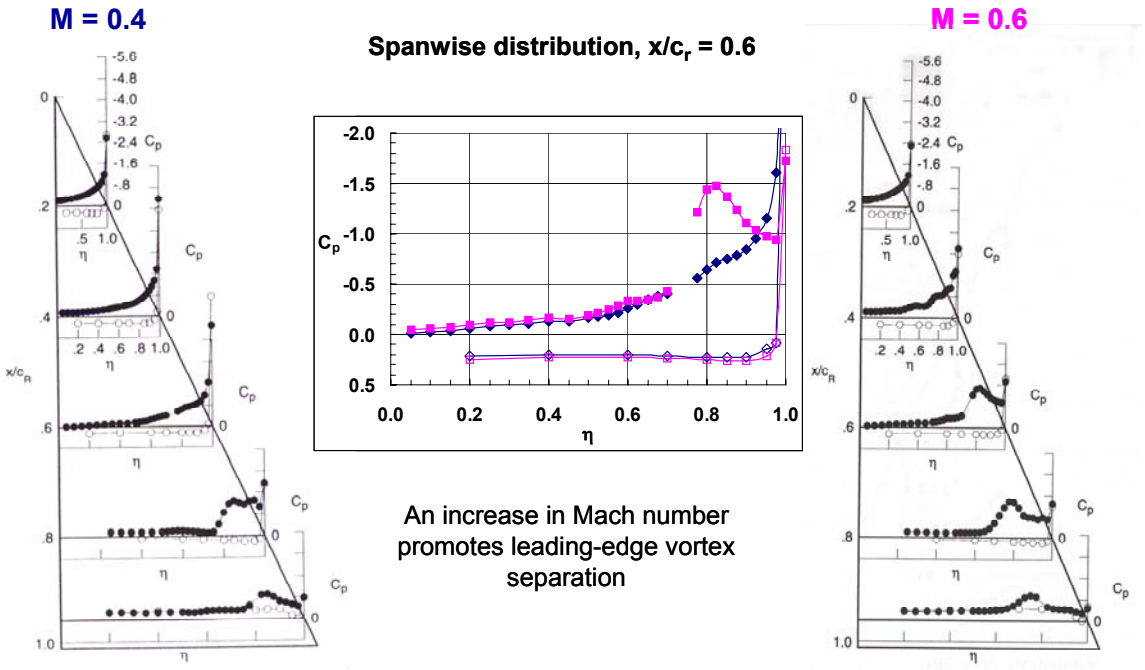

Figure 17. Effect of compressibility on static surface pressure coefficients. Medium bluntness, $\alpha = 13^o$, $R_{mac} = 60 \times 10^6$, data from NTF.

The compressibility effects on overall static surface pressures are shown in **Fig. 17** for the medium wing at an angle of attack of 13° and a Reynolds number of 60 million. The increase of mach number from 0.4 to 0.6 has show a significant increase in the extent of leading-edge vortex flow over the wing. For example, at the 60% chord station the pressure coefficients exhibit an essentially attached-flow trend at M = 0.4 whereas these pressure coefficients show a well-defined leading-edge vortex distribution at M = 0.6. There is also evidence of incipient separation at the 40% chord station for the higher Mach number results. Similar trends were found at the lower Reynolds number case (6 million).

D. Summary effects

The following three figures present a summary of the combined effects of Mach number, Reynolds number, leading-edge bluntness, and angle of attack for the onset and progression of leading-edge vortex separation. For this analysis the leading-edge pressure coefficients are used.

The effects of compressibility and bluntness on the leading edge pressure coefficients are presented in **Fig 18** at the mid-chord station for a Reynolds number of 6 million. Results are included only from the NTF experiments, and the medium bluntness leading edge results in this figure are the same as was shown in Fig. 16. The smaller bluntness leading edge only shows minimal compressibility effects although the trend (increase of Mach number promoting leading-edge separation) is sustained. Onset of separation is confined to a narrow angle of attack between 4° and 5°.

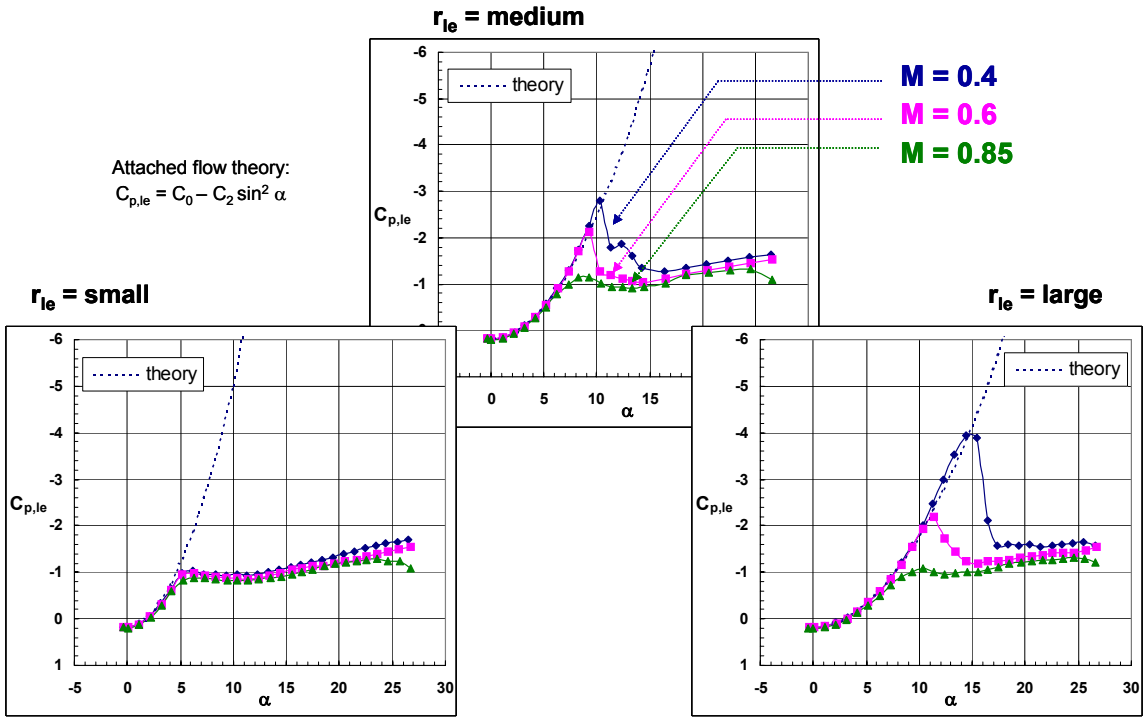

Figure 18. Compressibility and bluntness effects on leading-edge pressures. R_{mac} = 6 x 10^6, x/c_r = 0.5, data from NTF.

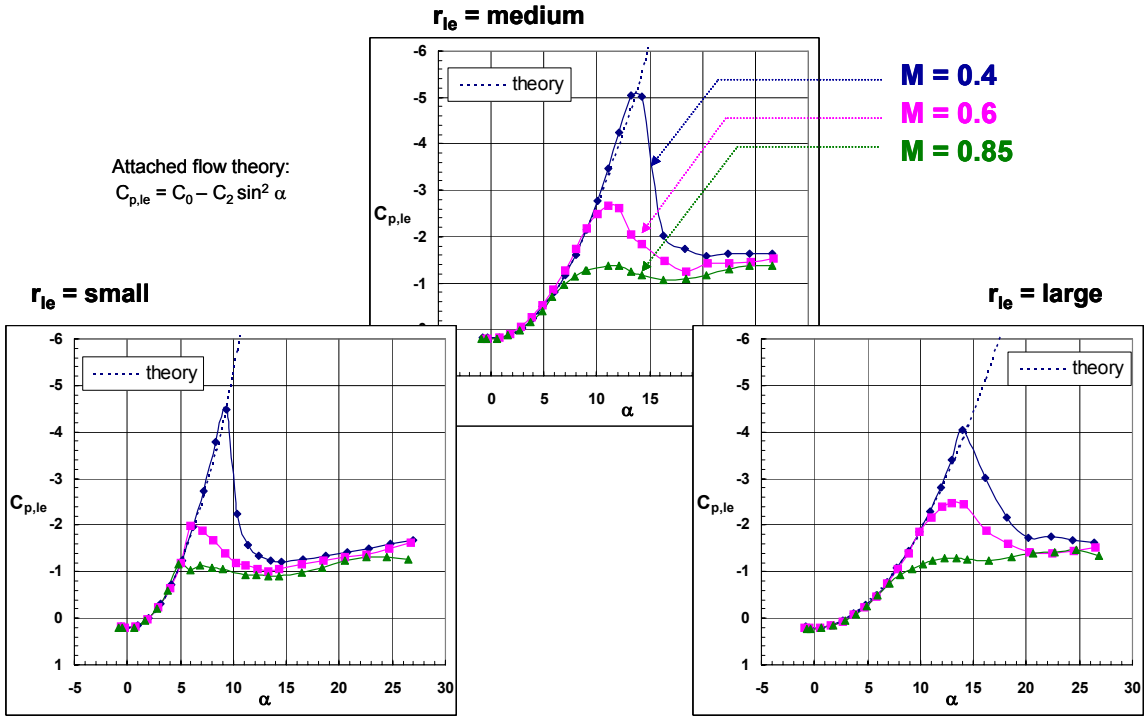

Figure 19. Compressibility and bluntness effects on leading-edge pressures. R_{mac} = 60 x 10^6, x/c_r = 0.5, data from NTF.

Results with the bluntest leading edge show that separation onset occurs at a higher angle of attack than the medium bluntness configuration. For example, at a Mach number of 0.4 the departure from the attached flow trend line shifts from about 11° for the medium bluntness wing to about 15.5° for the large bluntness wing. Similar compressibility trends are sustained for the blunt leading edge.

The same organization of results is presented in **Fig 19** but now for a Reynolds number of 60 million. At this Reynolds number, the small bluntness leading edge now exhibits significant compressibility effects consistent with the other data already discussed. Moreover, a comparison between Fig. 18 and Fig 19 demonstrate the delay in separation onset and progression with an increase in Reynolds number. Using the same example from the discussion of Fig. 18, the departure from the attached flow trend line for the medium bluntness leading edge at a mach number of 0.4 shifts from about 11° for the low Reynolds number case (Fig. 18) to about 14° for the high Reynolds number case (Fig. 19).

With the results shown in Fig. 18 and Fig. 19, as well as those from other wing stations or other free-stream flow conditions, the data from these experiments quantify the following trends:

(i) an increase in Reynolds number delays the onset and progression of blunt-leading-edge vortex separation,
(ii) an increase in Mach number promotes the onset and progression of blunt-leading-edge vortex separation,
(iii) an increase in angle of attack promotes the onset and progression of blunt-leading-edge vortex separation, and
(iv) an increase in leading-edge bluntness delays the onset and progression of blunt-leading-edge vortex separation.

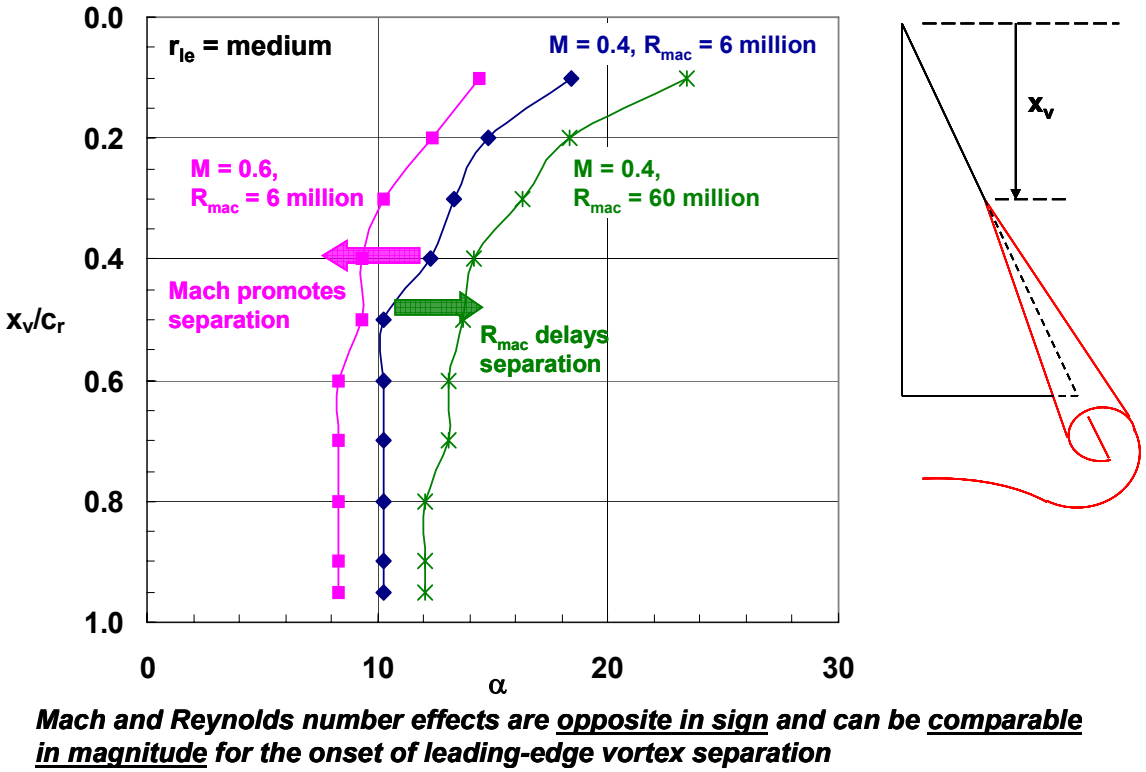

Figure 20. Compressibility and Reynolds number effects on onset and progression of leading-edge vortex separation. Medium bluntness, data from NTF

One summary example is shown in **Fig. 20** for the medium bluntness leading edge. The results presented are the inferred location of vortex separation from the leading edge pressure coefficients as a function of angle of attack. The baseline case in this figure is at a Mach number of 0.4 and a Reynolds number of 6 million. The data demonstrate first that, at a fixed Mach number, an increase in Reynolds number delays the onset and progression of leading-edge vortex separation. These results also demonstrate that, at a fixed Reynolds number, and increase in Mach number delays the onset and progression of leading-edge vortex separation. It is also noteworthy that the Mach and Reynolds number effects are not only opposite in sign but of comparable magnitude. If Reynolds number and Mach number were varied simultaneously, as would be the case in conventional atmospheric wind tunnel

testing, then the separate effects of compressibility flow physics and viscous flow physics would be confounded. These effects are sustained for the other leading edge bluntness values investigated.

V. Concluding Remarks

A summary has been presented of some initial experiments and analysis for separation-induced leading-edge vortex separation for a 65° delta wing that lead to the initiation of an international collaborative research effort known as Vortex Flow Experiment 2. The baseline experimentation from NASA Langley showed significant effects of Mach number, Reynolds number, angle of attack, and leading-edge bluntness for the onset and progression of leading-edge vortex separation. The data primarily included detailed static surface pressure distributions for a wide range of Reynolds numbers and Mach numbers taken in a manner that allowed for the isolation effects associated with these free-stream parameters.

The physics of blunt-leading-edge vortex separation fundamentally differs from the sharp-edged case in at least two regards. First, for the blunt leading edge the origin of the leading edge vortex is displaced from the apex of the delta wing. The onset and progression of this separation will be a function of flow conditions as well as leading-edge bluntness. Second, the existence of an inner, co-rotating vortex was inferred from the measurements. Neither of these phenomena occurs with the corresponding sharp leading edge. Both of these effects are quantified with the present data in terms as static surface pressure coefficients and limited force and moment coefficients.

However, it was clear that additional measurements would be required to better understand these effects. This need for new and more detailed data led to the VFE-2 experimental activities. The original experiments as well as the promise of new data sets also served as impetus for the computational program contained within VFE-2.

VI. References

[1]Wahls R A. The National Transonic Facility – A Research Retrospective. AIAA Paper 01-0754, January 2001.

[2]Luckring J M. An Overview of National Transonic Facility Investigations for High Performance Military Aerodynamics. AIAA Paper 01-0906, January 2001.

[3]Chu J, and Luckring J M. Experimental Surface Pressure Data Obtained on 65° Delta Wing Across Reynolds Number and Mach Number Ranges. Volume 1 – Sharp Leading Edge, *NASA TM-4645*, February 1996.

[4]Chu J, and Luckring J M. Experimental Surface Pressure Data Obtained on 65° Delta Wing Across Reynolds Number and Mach Number Ranges. Volume 2 – Small Leading Edge, *NASA TM-4645*, February 1996.

[5]Chu J, and Luckring J M. Experimental Surface Pressure Data Obtained on 65° Delta Wing Across Reynolds Number and Mach Number Ranges. Volume 3 – Medium Leading Edge, *NASA TM-4645*, February 1996.

[6]Chu J, and Luckring J M. Experimental Surface Pressure Data Obtained on 65° Delta Wing Across Reynolds Number and Mach Number Ranges. Volume 4 – Large Leading Edge, *NASA TM-4645*, February 1996.

[7]Luckring J M. Reynolds Number and Leading-Edge Bluntness Effects on a 65° Delta Wing. AIAA Paper 2002-0419, January 2002.

[8]Luckring J M. Transonic Reynolds Number and Leading-Edge Bluntness Effects on a 65° Delta Wing. AIAA Paper 2003-0753, January 2003.

[9]Luckring J M. Compressibility and Leading-Edge Bluntness Effects on a 65° Delta Wing. AIAA Paper 2004-765, January 2004.

[10]Luckring J M. Reynolds Number, Compressibility, and Leading-Edge Bluntness Effects on Delta Wing Aerodynamics. ICAS Paper ICAS04-414, September 2004.

[11]Hummel D, and Luckring J M. Private discussions. 2001.

[12]Hummel D. and Redeker G. A New Vortex Flow Experiment for Computer Code Validation. *RTO MP-069*, Paper No. 9, March 2003.

[13]Hummel D. On the Vortex Formation Over a Slender Wing at Large Incidence. *AGARD CP-247*, Paper No. 15, January 1979.

[14]Polhamus E C. A Concept of the Vortex Lift of Sharp-Edged Delta Wings Based on a Leading-Edge Suction Analogy. *NASA TN D-3767*, 1966.

[15]Fuller D E. Guide for Users of the National Transonic Facility. *NASA TM-83124*, 1981.

[16]Foster J M, and Adcock J B. Users Guide for the National Transonic Facility Research Data System. *NASA TM-110242*, April 1996.

[17]Mcghee R J, Beasley W D, and Foster J M. Recent Modifications and calibration of the Langley Low-Turbulence Pressure Tunnel. *NASA TP-2328*, July 1984.

[18]Frink N T. Computational Study of Wind-Tunnel Wall Effects on Flow Field Around Delta Wings. AIAA Paper 87-2420, pp 381-391 in *Proceedings of the AIAA 5th Applied Aerodynamics Conference*, 1987.

[19]Frink N T. Wind Tunnel Wall Effects on Delta Wings. *AIAA J. Aircraft*, Vol. 26, No. 5, pp 403-404, May 1989.